Available online at www.sciencedirect.com
SCIENCE DIRECT®
ELSEVIER
Nuclear Instruments and Methods in Physics Research A 550 (2005) 116–126
NUCLEAR INSTRUMENTS & METHODS IN PHYSICS RESEARCH Section A
www.elsevier.com/locate/nima

Cosmic ray tests of double-gap resistive plate chambers for the CMS experiment

M. Abbrescia[a], E. Cavallo[a], A. Colaleo[a], G. Iaselli[a], F. Loddo[a], M. Maggi[a,*], B. Marangelli[a], S. Natali[a], S. Nuzzo[a], G. Pugliese[a], A. Ranieri[a], F. Romano[a], R. Trentadue[a], N. Cavallo[c], G. Comunale[c], P. Paolucci[c], D. Piccolo[c], C. Sciacca[c], G. Belli[b], C. De vecchi[b], R. Guida[b], S.P. Ratti[b], C. Riccardi[b], P. Torre[b], P. Vitulo[b], Y. Ban[d], J. Cai[d], H. Liu[d], S. Qian[d], Q. Wang[d], Y. Ye[d], J. Ying[d], A. Dimitrov[e], I. Glushkov[e], L. Litov[e], I. Nasteva[e], B. Pavlov[e], P. Petkov[e], T. Anguelov[f], V. Genchev[f], P. Iaydjiev[f], B. Panev[f], S. Stoykova[f], G. Sultanov[f], R. Trayanov[f], P. Vankov[f]

[a]*Dipartimento Interateneo di Fisica and Sezione INFN, Bari, Italy*
[b]*Dipartimento di Fisica Nucleare e Teorica and Sezione INFN, Pavia, Italy*
[c]*Dipartimento di Fisica Nucleare e Teorica and Sezione INFN, Napoli, Italy*
[d]*Peking University, China*
[e]*Atomic Physics Department, Faculty of Physics, University of Sofia, Bulgaria*
[f]*INRNE, BAS, Sofia, Bulgaria*

Received 11 April 2005; received in revised form 2 June 2005; accepted 8 June 2005

Abstract

The CMS Barrel resistive plate chambers quality tests are performed at three different sites (Bari, Pavia and Sofia), where equivalent software and hardware tools are used. Data from the first 210 detectors are available for a comprehensive analysis. The paper describes the general experimental set-up, the test procedure and the cosmic muon test results. The muon trajectory reconstruction algorithm, used for precise studies, is presented. The criteria to accept or reject a detector are also given. The CMS final-design chambers show an average efficiency greater than 95%.

PACS: 29.40.C

Keywords: RPC; Muon system; CMS; Trigger

*Corresponding author. Tel.: +39 080 5442181.
E-mail address: Marcello.Maggi@ba.infn.it (M. Maggi).

0168-9002/$ - see front matter © 2005 Elsevier B.V. All rights reserved.
doi:10.1016/j.nima.2005.06.074

1. Introduction

Future CERN LHC experiments will adopt resistive plate chambers (RPC) in their trigger systems [1–3]. RPCs [4] are gaseous parallel-plate detectors with time resolution competitive to that of scintillators (~1 ns) and good spatial resolution (~1 cm) [2]. Signals are induced on a read-out stripped plane outside the gas volume.

The basic constituent of the CMS RPC chamber is the so-called *single-gap*. It is made of two parallel high-resistivity bakelite plates ($\sim 10^{10}\,\Omega$ cm) which form a 2 mm gas gap. In particular, CMS will use double-gap RPCs [1] operated in avalanche mode (reduced gas gain) [2] to ensure high rate capability (~1 kHz/cm^2). A *double gap* consists of two *single gap*s put one on top of the other with common read-out copper strips in the middle. The signal is induced by the two avalanches simultaneously leading to an improved detection efficiency [5] being the sum of two *single gap* signals.

Each Barrel chamber consists of two *double gap*s, named forward (FW) and backward (BW). These are held together by aluminum profiles.

Among all 480 chambers foreseen to complete the entire Barrel RPC system more than 200 have already been accepted.

2. Experimental set-up

The experimental areas for RPC cosmic ray tests are located in Bari (Physics Department and INFN unit), Pavia (Physics Department and INFN unit) and Sofia (INRNE) [6]. Special halls are equipped with cranes, low- and high-voltage power supplies, gas-distribution lines, weather stations and data acquisition systems.

Cosmic ray test facilities are operational in all sites. They consist of metallic towers where chambers can be placed horizontally and read out in coincidence with the passage of triggering muons. A maximum of ten chambers at Bari site and five at Pavia and Sofia sites can be tested simultaneously. Temperature in the halls is kept constant by an air-conditioning systems.

The experimental set-up for one cosmic ray muon test stand consists of a muon trigger system that is provided by a set of scintillators located on the top and bottom of the test tower. It is based on two double layers of scintillators covering an area of $125 \times 44\,\text{cm}^2$. Fig. 1 shows the scintillator locations: S1, S2 on top and S3, S4 at the bottom of the tower. They are all connected in logical AND. Small ($60 \times 40\,\text{cm}^2$) plastic scintillators, V1 and V2, which are placed on the top of the tower at a distance of 50 cm from the muon trigger system, are also used to veto electromagnetic showers. The overall trigger signal, used after noise discrimination, follows the logic $T = (S1 \cap S2 \cap S3 \cap S4) \cap (\overline{V1 \cup V2})$. The trigger system is supported by a mechanical structure which allows one-dimensional displacement of the scintillators along the strip length to cover either the FW or the BW part of a chamber.

The gas system is based on a series of three *Bronkhorst Hi-Tec* EL-FLOW® mass flow meter/controllers F-201C. The gas mixture is composed of 96.2% $C_2H_2F_4$, 3.5% *iso*-C_4H_{10} and 0.3% SF_6 and it is distributed via parallel system to the chambers. Water vapors are also added to humidify the operating gas within 40–45%. The gas composition is monitored and known with a relative precision better than 1%.

The High-voltage (HV) power supply distribution is based on the Universal Multichannel CAEN-SY1527 unit which has internal processor and network connection. A dedicated

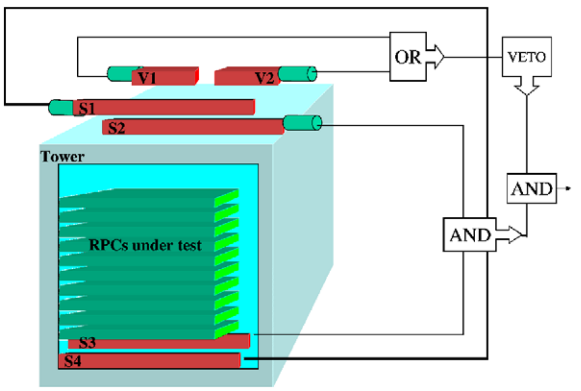

Fig. 1. Experimental set-up and trigger logic scheme.

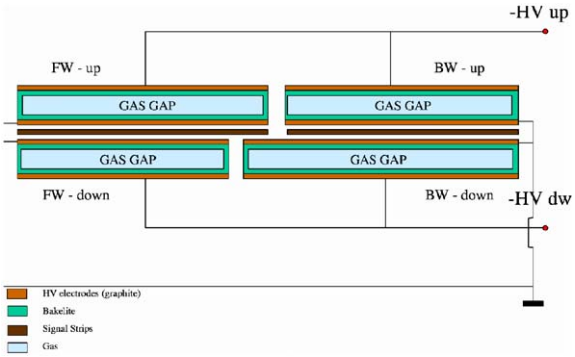

Fig. 2. High-voltage supply diagram.

software (with graphical user interface) is developed to monitor the high-voltage channels and selectively record the values. Each chamber is supplied by two HV channels, as shown in Fig. 2. One high-voltage channel supplies a complete *single-gap* layer, UP or DOWN, consisting of both (FW and BW) gaps.

The low-voltage system is ensured by EUTRON GCTR modules. It supplies internal dedicated *Distribution Boards* which feed all front-end electronics and distribute slow control signals via I^2C bus. Kapton foils are used to connect read-out strips to *Front-End Boards* (FEB) [7]. The latter form LVDS signals after amplification and discrimination, which are further processed by the data acquisition system (DAQ).

The DAQ consists of two VME crates housing thirty 64-channel TDC modules sampled by a 40 MHz clock (which corresponds to 25 ns time sensitivity). Each TDC processes the LVDS signals coming from four FEBs. TDCs are programmed in a "common stop" configuration. When the trigger arrives the data is transmitted to a PC for storage and analysis.

The values of humidity, temperature and pressure are monitored by Oregon Scientific-WMR918-Weather Station. The sensors continuously transmit data via radio signal to the base station which is connected to a PC by RS-232 serial interface. The values are stored once per minute.

A summary of the chamber performance is stored into the RPC Production Database,[1] which is based on MySQL, together with all the information about the environmental conditions. Data for each chamber are accessible through a web interface. PHP scripts and JAVA applets are used to display summary plots.

3. Results

The main parameters of the RPCs are dark current, efficiency, noise rate and cluster size. Both *single-* and *double-gap* running modes are studied to control the quality of the chamber performance.

A preliminary calibration of the data is necessary in order to take into account different atmospheric conditions in the different sites and along the test duration. The applied high voltage value HV_{app} is corrected for temperature and pressure variation (P–T correction) according to [8]:

$$HV_{eff} = HV_{app}\frac{P_0}{P}\frac{T}{T_0} \quad (1)$$

to give an effective high voltage HV_{eff}, where T_0 (293 °K) and P_0 (1010 mbar) are the reference temperature and pressure. The average atmospheric pressure in Bari, Pavia and Sofia are respectively 1010, 1005 and 950 mbar, while the temperature is kept stable at 20–21 °C by heating fans. On average the correction spread is of the order of 1%. The maximum observed variation is 3% due to winter–summer differences.

After calibration, values of current (for a given layer), noise rate and cluster size (for a given *double gap*) are fitted by means of a second order polynomial in the range of $HV_{eff} = [9.0, 9.8]$ kV, to establish the functional relationship of those parameters in the relevant operating region. For efficiency, data is fitted by a sigmoid function of the type:

$$\varepsilon = \frac{\varepsilon_{max}}{1 + e^{S(HV_{eff} - HV_{50\%})}}, \quad (2)$$

[1] http://webcms.ba.infn.it/rpc

where the parameter ε_{max} represents the maximum plateau efficiency, $HV_{50\%}$ is the HV_{eff} at 50% of the maximum efficiency and S is proportional to the slope of the efficiency curve at $HV_{50\%}$. Typical experimental points and fits superimposed on are shown in Fig. 3.

3.1. Dark current

Distributions of the dark current for both layers at $HV_{eff} = 9.6\,kV$, as obtained from the fit to the data, are shown in Fig. 4. A convention to reject a *single-gap* layer with a current exceeding 10 μA is to be followed. The chambers that do not fulfill this requirement are closely monitored. All *double gaps* drawing most of the current are replaced and the chambers are to be retested.

3.2. Efficiency

Chamber efficiency is obtained with the "coincidence" method by evaluating the ratio between the number of events in which RPC has at least one fired strip in the trigger window (100 ns) and the total number of recorded events. A correction for spurious hits is also applied [9].

On Fig. 5 the distributions of the maximum *double-gap* efficiency are plotted for the three sites. The difference is due to a different geometrical acceptance of various chambers with respect to trigger area cross section. The mean value of the distribution is 97.2%. Chambers with efficiency less than 90% are not accepted.

In Fig. 6 the HV_{eff} distributions for *single-* and *double gaps* are shown for different efficiencies (50%, 90%, 95%) relative to the maximum

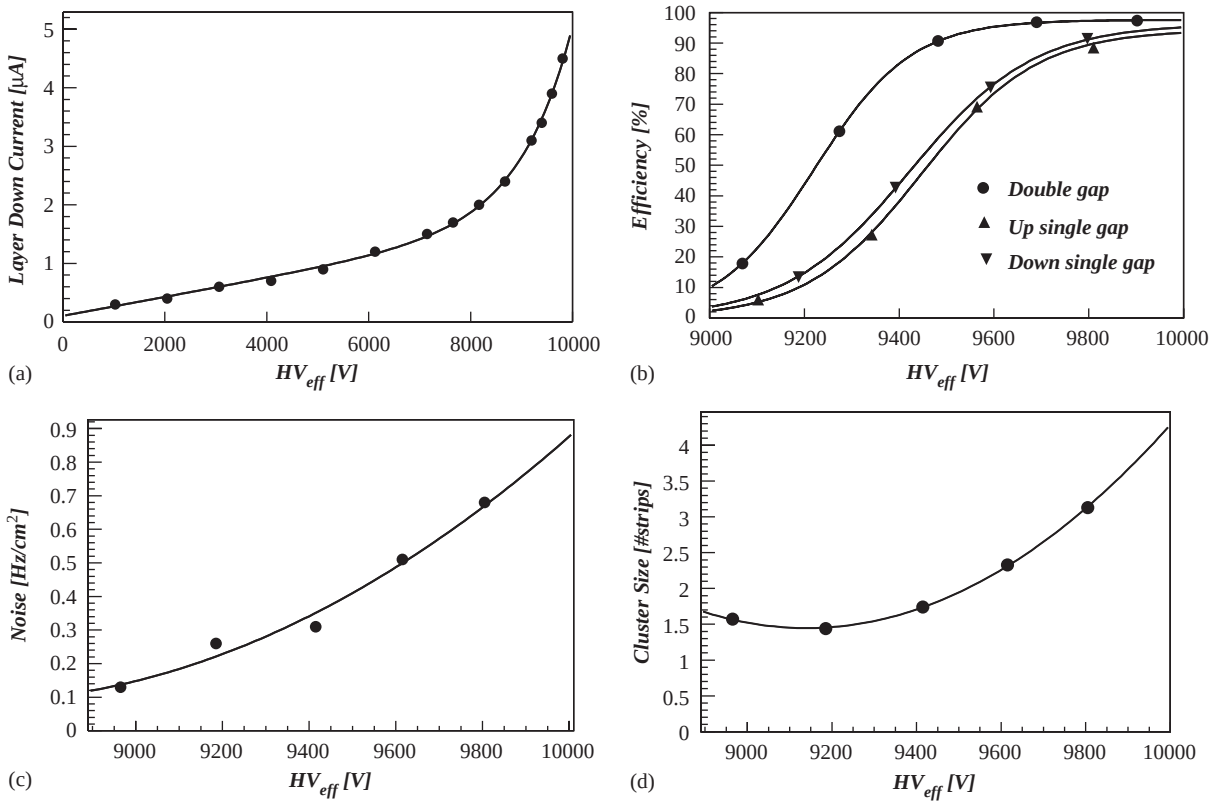

Fig. 3. Main parameters under investigation: current vs HV (a), *single-* and *double-gap* efficiency vs HV (b), noise hit rate vs HV (c), cluster size vs HV (d).

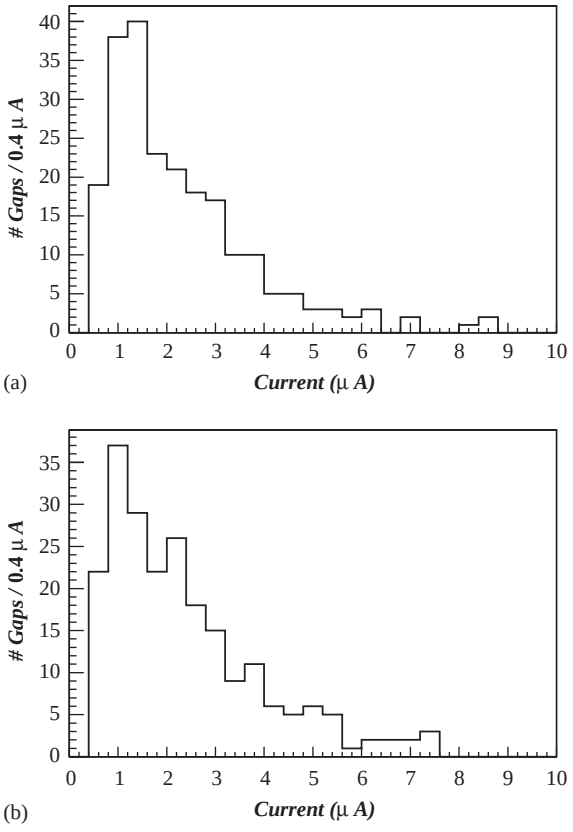

Fig. 4. Current distributions for layers up (a) and down (b) at $HV_{eff} = 9.6\,kV$.

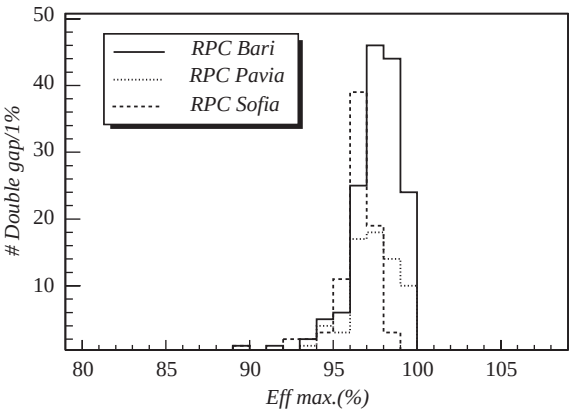

Fig. 5. Distribution of the maximum *double-gap* efficiency.

efficiency. The point corresponding to 95% of the maximum efficiency is named as the "knee" of the efficiency curve. As expected, for a given efficiency,

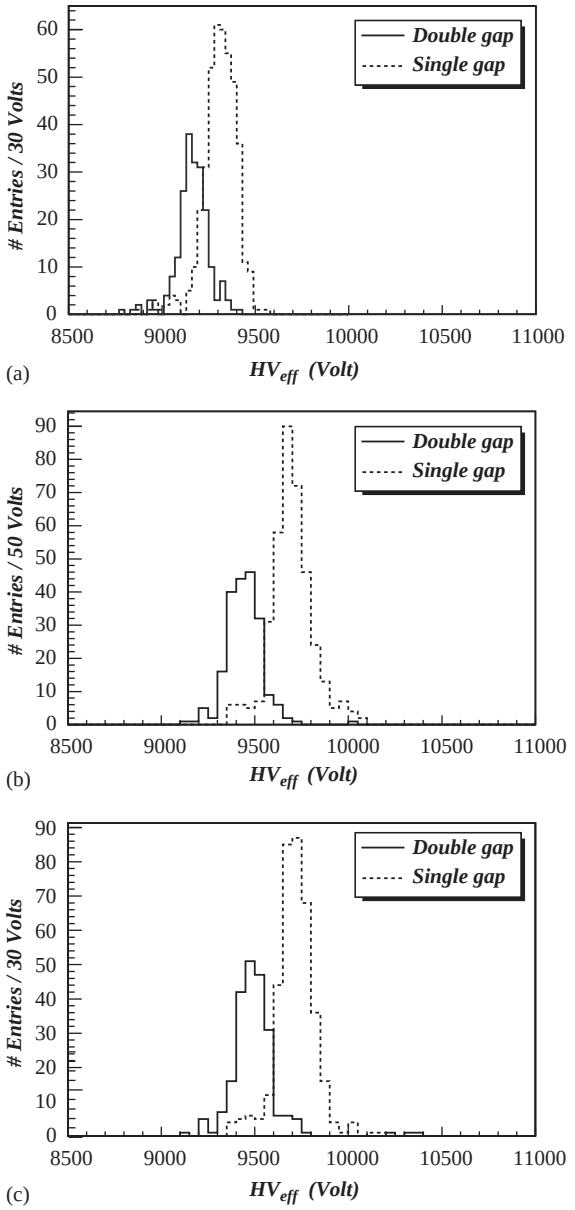

Fig. 6. Effective high voltage (HV_{eff}) distribution at 50% maximum efficiency (a), HV_{eff} distribution at 90% maximum efficiency (b), HV_{eff} distribution at 95% maximum efficiency (c).

the *double-gap* configuration operating voltage is lower than that corresponding to the *single-gap* running mode.

Each chamber is also characterized by the slope of the efficiency curve as a function of the supplied

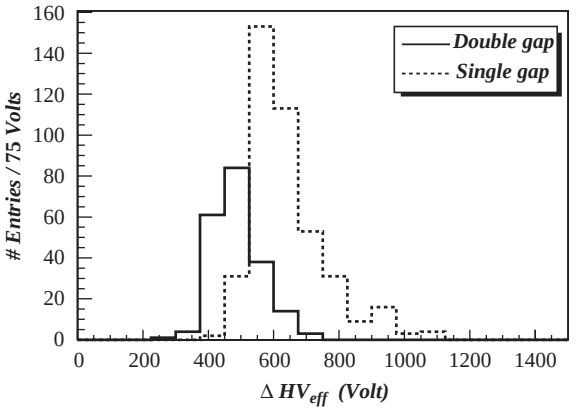

Fig. 7. $\Delta^{90\%}_{10\%}$ distribution for *single-* and *double-gap*.

high voltage. It is evaluated as the high voltage difference, $\Delta^{90\%}_{10\%}$, between the efficiency points at 90% and 10% relative to ε_{max}. From Eq. (2) it follows that $\Delta^{90\%}_{10\%}$ is proportional to $1/S$.

The distribution of $\Delta^{90\%}_{10\%}$ is shown in Fig 7. The *double-gap* design has smaller $\Delta^{90\%}_{10\%}$ spread which corresponds to a better homogeneity in the chamber behaviour. During the tests, the forward and backward gaps are supplied by a common HV channel (Fig. 2). It is therefore important to measure forward–backward homogeneity. The distribution of forward–backward difference of the high voltage at the "knee", in *double-gap* configuration, is shown in Fig. 8.

On average, less than 100 V beyond the "knee" are necessary to bring the entire chamber in full efficiency.

3.3. Noise rate

The noise rate is defined as the number of fired strips per second outside the trigger window, normalized to the surface of the strips. Threshold control on front-end electronic discriminators gives the possibility to set efficiency and noise rate in the proper limits. A noise rate up to 10 Hz/cm^2 is considered acceptable.

Whenever the rate becomes high only for a few strips in a chamber a careful investigation often leads to a substitution of a faulty FEB. The average chamber noise rate is evaluated by masking the strips with a hit rate larger than 20 Hz/cm^2. Fig. 9 illustrates the distribution of masked strips in the analyzed chamber sample. The resulting distribution of average noise rate after strip masking is shown in Fig. 10 at the operating voltage of 9.6 kV. The tested chambers have an average noise rate less than 5 Hz/cm^2.

3.4. Cluster size

All simultaneously fired adjacent strips form a cluster. The dimension of the cluster is called cluster size. The cluster size of a chamber is defined as the average value of the cluster size distribution,

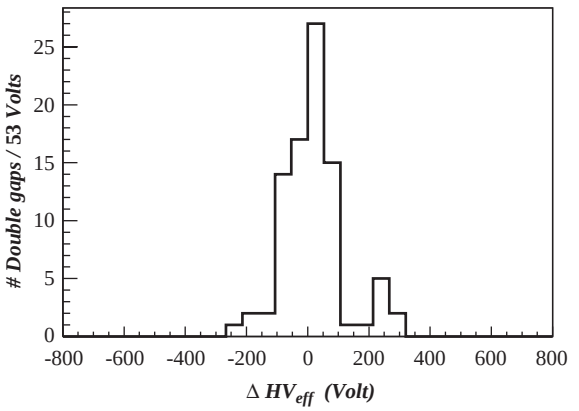

Fig. 8. Distribution of the difference between the high voltage values at the knees of the forward and backward *double gaps*.

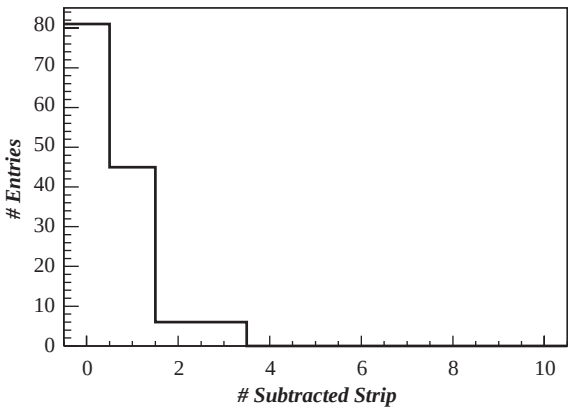

Fig. 9. Number of eliminated strips in a chamber with a noise rate greater than 20 Hz/cm^2.

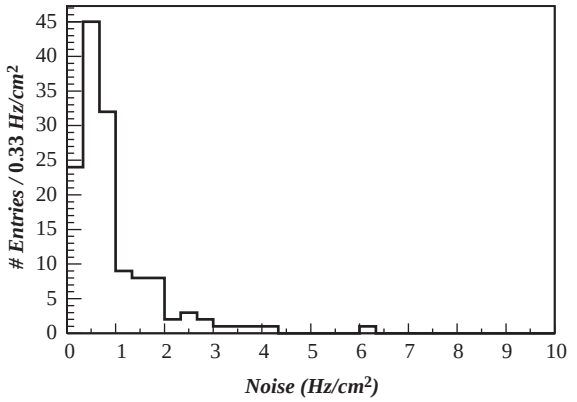

Fig. 10. Noise hit rate for double gaps at 9600 V.

sampled in the first 25 ns of the trigger window (100 ns).

The chamber cluster size distribution for all tested *double gaps* at a fixed voltage ($HV_{eff} = 9.6$ kV) is shown in Fig. 11(a). Since the chambers have different operating voltages, the chamber cluster size distribution at voltages corresponding to the knee of the efficiency is also shown in Fig. 11(b). As expected, the last distribution is significantly narrower than the distribution at the fixed voltage.

The dependence of the chamber cluster size distribution on the effective voltage is presented in Fig. 12 as a profile histogram. The dots represent the averages of the chamber cluster size distributions at different HV_{eff} while the bars are their root mean squares.

3.5. Crosstalk

As already described, the CMS RPC detectors consist of two *double gaps*, read out by separate strip planes. In order to avoid ambiguities in the track reconstruction in the trigger system, it is essential to ensure that the level of *crosstalk* between the two strip planes remains negligible.

The *crosstalk* is measured as the fraction of events in which both FW and BW *double gap* are fired in the trigger window. Moreover, the involved strips are required to be either geometrically corresponding or those adjacent to them. To distinguish *crosstalk* from signals induced by

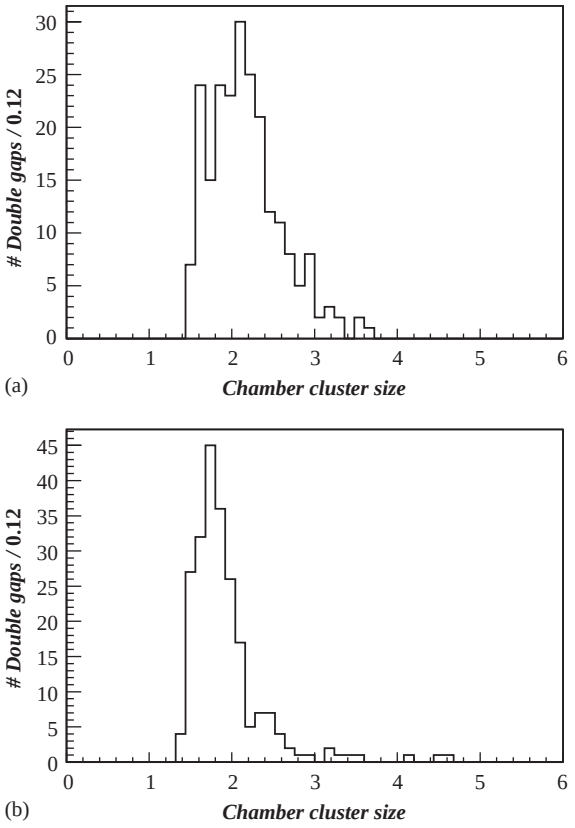

Fig. 11. Chamber cluster size distribution at $HV_{eff} = 9.6$ kV (a) and chamber cluster size distribution at the knee of the efficiency curve (b).

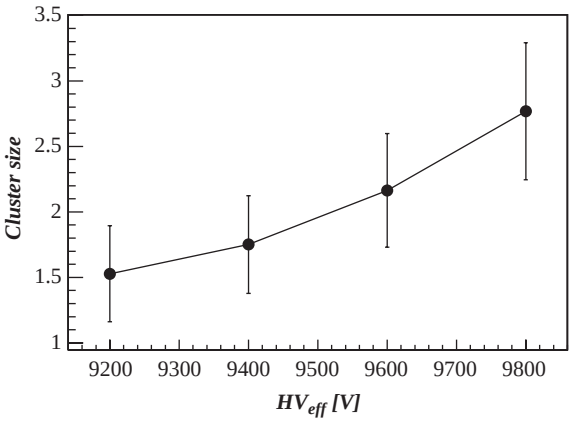

Fig. 12. Profile histogram of the chamber cluster size distribution as a function of effective voltage. The dots and bars are, respectively, the average and root mean squares of the distributions.

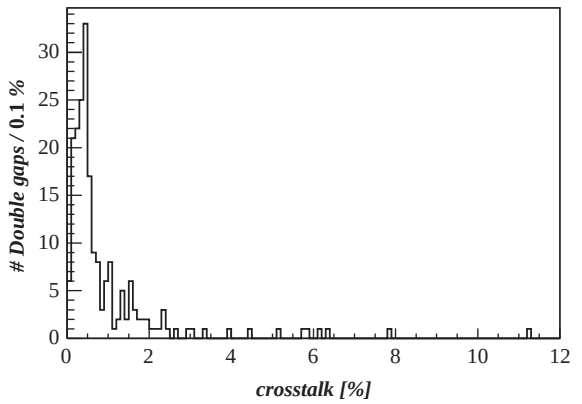

Fig. 13. *Crosstalk* distribution between FW and BW *double gaps* at an operating voltage of 9.8 kV. Here the trigger system ensures that only the FW region is covered by the trigger.

cosmic showers or electronic noise, only events with strip multiplicity smaller than six are considered. The *crosstalk* distribution at an operating voltage of 9.8 kV for the chambers is reported in Fig. 13.

4. Muon reconstruction

A muon reconstruction software is developed to achieve higher accuracy in efficiency measurements and study local properties of the chambers. The test stand geometry allows a reconstruction of tracks in a two-dimensional view, where the X-coordinate is defined by the strip position along the chamber and the Y-coordinate by the chamber position in the tower. In the following section only data taken at Bari site are considered, since in Pavia and Sofia the number of chambers, tested simultaneously, has never exceeded four, which makes the reconstruction algorithm not fully reliable. The procedure applied to each event is described below.

4.1. Pattern recognition

The fired strips are clustered. The barycenter, identified by (x,y) coordinates, and the size are computed for each cluster. If more than three clusters with size greater than six are present in the telescope, the event is considered as a "shower" and it is rejected.

A muon trajectory is parameterized by

$$X = B - (\mathrm{tg}\,\alpha)\,Y.$$

For each pair of clusters (x_i,y_i) and (x_j,y_j), belonging to different chambers, a pair of parameters $(\mathrm{tg}\,\alpha_{ij}, B_{ij})$ is assigned, according to the formulas:

$$\mathrm{tg}\,\alpha_{ij} = \frac{x_i - x_j}{y_i - y_j}$$

$$B_{ij} = x_i + \frac{x_i - x_j}{y_i - y_j}\,y_i$$

Each pair of clusters gives an entry into a two-dimensional histogram $(\mathrm{tg}\,\alpha, B)$. Pairs lying on a straight line have similar $\mathrm{tg}\,\alpha$ and B and give entries to one or few adjacent histogram bins. Thus, the trajectory candidate can be determined by means of the histogram $(\mathrm{tg}\,\alpha, B)$ by selecting the clusters present in the bin with maximum number of entries.

In order to eliminate triggers not induced by single-muon events, a clear example of which is illustrated on Fig. 14, only trajectories which cross the trigger scintillators are considered.

One chamber is chosen as a test chamber and the others serve as reference ones. Successfully reconstructed trajectories are required to have

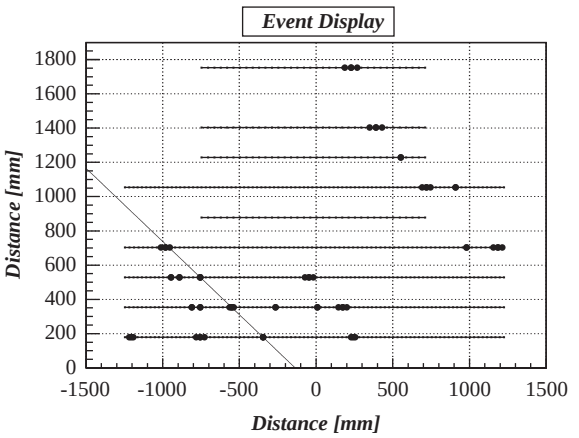

Fig. 14. Display of a multi-muon event. The trigger is given by two different muons.

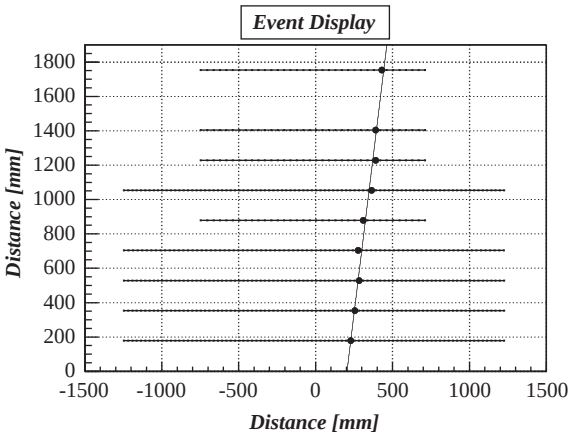

Fig. 15. Display of a reconstructed single-muon event.

clusters at least in four reference chambers. Only clusters in the reference chambers are used. A typical reconstructed muon event is shown in Fig. 15.

4.2. Analysis and results

A detailed analysis of chamber performance can be carried out using the reconstructed trajectories. The reconstruction is applied to a sample of 200 chambers at the operating voltages of 9.6 and 9.8 kV, to ensure that the detectors are fully efficient.

4.3. Global properties

After the reconstruction, the track impact point on the chambers under test is determined. A typical distribution of the difference between the impact point and the nearest cluster center in one chamber, with 27.3 mm strip width, is plotted on Fig. 16.

The root mean square of the distribution represents the spatial resolution of the chamber, since the error on the track impact point is expected to be negligible. As shown, the resolution is clearly dominated by the strip width.

The mean value of the residual distribution represents an offset, which is used in the realignment procedure, implemented for better performance of the pattern recognition.

Chamber global efficiency is now evaluated by using the reconstructed trajectories. If a reconstructed muon trajectory goes through a fired strip or its neighbor, the chamber is considered efficient. Efficiencies obtained by the reconstruction and the "coincidence" method (Para 3) at the fixed voltages of 9.6 and 9.8 kV are plotted on Figs. 17 and 18. As can be observed, the computed efficiencies from the muon reconstruction are few percent higher than those determined by the "coincidence" method. This is due mainly to multi-muon events that are not rejected with the latter method.

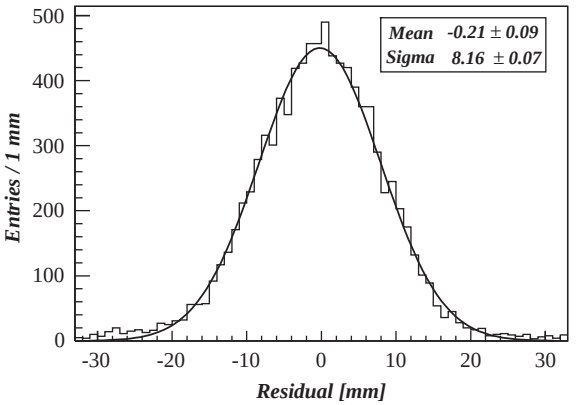

Fig. 16. Gaussian fit on residual distribution.

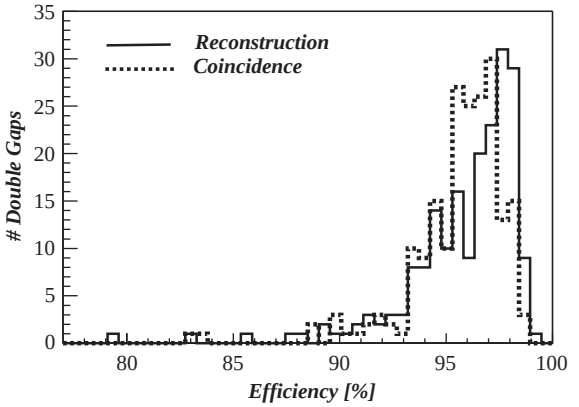

Fig. 17. Efficiency obtained by reconstruction and "coincidence" method at 9.6 kV.

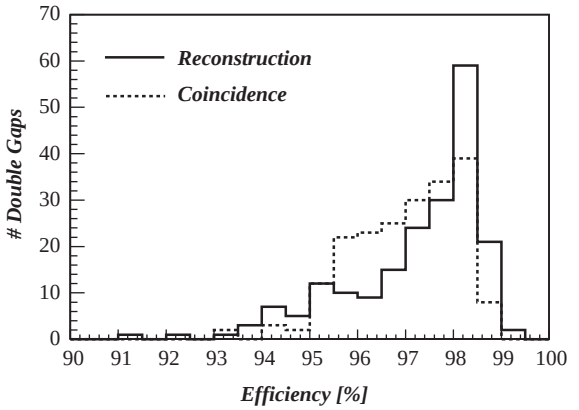

Fig. 18. Efficiency obtained by reconstruction and "coincidence" method at 9.8 kV.

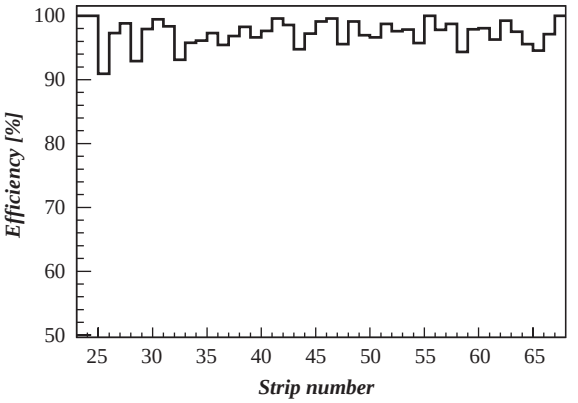

Fig. 19. Strip-by-strip efficiency.

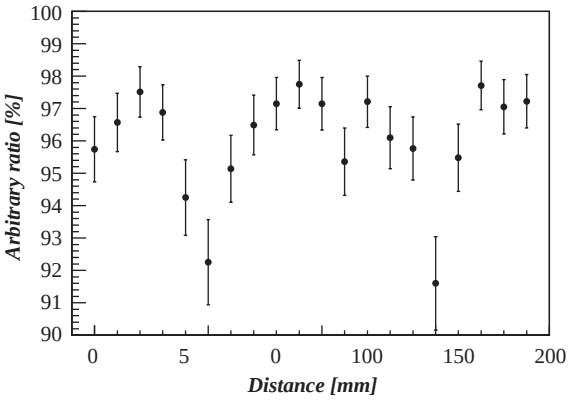

Fig. 20. Local efficiency. The chamber is subdivided in 200 mm slices which are superimposed. The distance between two inefficient areas matches the distance between spacers.

4.4. Local properties

The determination of the muon impact point position allows the study of the chamber efficiency, defined above, for each strip along the X direction. A typical plot of local strip efficiency is given on Fig. 19. The efficiency is uniform over the investigated region.

One may expect regions with lower local efficiency due to spacers. However, this effect is very small. The spacers are cylindrical objects (0.8 cm in diameter) glued to the bakelite plates to form the knots of a 100 mm square grid. In order to increase the statistics and emphasize on the spacer effect, data samples from different 200 mm regions of a chamber are aligned and superimposed on one single plot in Fig. 20. Inefficient areas and spacer sizes are in good agreement. The distance between adjacent inefficient regions matches the spacer pitch.

5. Conclusions

About 250 CMS Barrel Resistive Plate chambers are produced and 210 of them are tested with cosmic muons. Dedicated test procedure is established and trajectory reconstruction software is developed. During the tests dark current is monitored and efficiency, cluster size and noise rate are measured. Less than 5% of the chambers are rejected for low efficiency and high current. All accepted chambers show high efficiency ($>95\%$), acceptable clusters size (average value $\sim$2.5 strips) and low noise ($<5\,\mathrm{Hz/cm^2}$).

Acknowledgements

The authors are greatly indebted to all technical and engineering staff for their important contribution to the design and testing activities. We are grateful for their dedicated work and we are aware that the successful construction of the CMS RPC Barrel system will depend, also, on their skills and commitment. A special mention goes to A. Clemente and K. Abadjiev for their important

contribution to the design of the test stands and assembling tables.

References

[1] CMS Collaboration, Technical Proposal, CERN/LHCC 94–38, 15 December 1994.
[2] CMS Collaboration, Muon Project, CERN/LHCC 97–32, 15 December 1997.
[3] ATLAS Muon Collaboration, ATLAS Muon Technical Design Report, CERN/LHCC 97–22, 5 June 1997.
[4] R. Santonico, R. Cardarelli, Nucl. Instr. and Meth. 187 (1981) 377.
[5] M. Abbrescia, et al., Nucl. Instr. and Meth. A 431 (1999) 413 and references there in.
[6] T. Angelov, et al., Test set-up for the CMS resistive plate chambers, Meetings in Physics at University of Sofia 3 (2002) 73.
[7] M. Abbrescia, et al., Nucl. Instr. and Meth. A 456 (2000) 143.
[8] M. Abbrescia, et al., Nucl. Instr. and Meth. A 394 (1997) 341.
[9] M. Maggi, Sci. Acta 13 (1998) 139.